

# 1 Learning in visual regions as support for the 2 bias in future value-driven choice

3 Sara Jahfari<sup>\*1,2</sup>, Jan Theeuwes <sup>3</sup>, Tomas Knapen <sup>1,3</sup>

4  
5 <sup>1</sup> Spinoza Centre for Neuroimaging, Royal Netherlands Academy of Arts and Sciences  
6 (KNAW), The Netherlands

7 <sup>2</sup> Department of Psychology, University of Amsterdam, The Netherlands

8 <sup>3</sup> Department of Experimental and Applied Psychology, Vrije Universiteit van Amsterdam,  
9 The Netherlands

## 10 **Abstract**

11 Reinforcement learning can bias decision-making towards the option with the highest expected  
12 outcome. Cognitive learning theories associate this bias with the constant tracking of stimulus values and  
13 the evaluation of choice outcomes in the striatum and prefrontal cortex. Decisions however first require  
14 processing of sensory input, and to-date, we know far less about the interplay between learning and  
15 perception. This fMRI study (N=43), relates visual BOLD responses to value-beliefs during choice, and,  
16 signed prediction errors after outcomes. To understand these relationships, which co-occurred in the  
17 striatum, we sought relevance by evaluating the prediction of future value-based decisions in a separate  
18 transfer phase where learning was already established. We decoded choice outcomes with a 70% accuracy  
19 with a supervised machine learning algorithm that was given trial-by-trial BOLD from visual regions  
20 alongside more traditional motor, prefrontal, and striatal regions. Importantly, this decoding of future  
21 value-driven choice outcomes again highlighted an important role for visual activity. These results raise  
22 the intriguing possibility that the tracking of value in visual cortex is supportive for the striatal bias  
23 towards the more valued option in future choice.

24  
25 **Keywords:** Bayesian hierarchical modelling, decoding, random forest machine learning, reinforcement  
26 learning, perceptual learning

---

\*Corresponding author: sara.jahfari@gmail.com

27

28 In decision-making, our value beliefs bias future choices. This bias is shaped by the outcomes of similar  
29 decisions made in the past where the action, or stimulus chosen, becomes associated with a positive or  
30 negative outcome ('value beliefs'). The evaluation of value after an outcome, or the comparison of value in  
31 decisions, is traditionally associated with activity in the prefrontal cortex and striatum (O'Doherty et al.  
32 2004, 2017; Daw et al. 2006; Kahnt et al. 2009; Hare et al. 2011; Jocham et al. 2011; Klein et al. 2017).  
33 To underset the bias in action selection midbrain dopamine neurons are thought to send a teaching signal  
34 towards the striatum and prefrontal cortex after an outcome (Montague et al. 1996; Schultz et al. 1997;  
35 Tobler et al. 2005). In the striatum, future actions are facilitated by bursts in dopamine after positive  
36 outcomes or discouraged by dopamine dips after negative outcomes. The dorsal and ventral parts of the  
37 striatum are known to receive differential, but also overlapping, inputs from midbrain neurons (O'Doherty et  
38 al. 2004; Atallah et al. 2007). Ventral and dorsal striatum have also been ascribed a differential role during  
39 learning by reinforcement learning theories. Here, the ventral parts of the striatum are involved with the  
40 prediction of future outcomes through the processing of prediction errors, whereas the dorsal striatum uses  
41 the same information to maintain action values as a way to bias future actions towards the most favored  
42 option (Joel et al. 2002; Kahnt et al. 2009; Collins and Frank 2014). Intriguingly, however, before many  
43 of these value-based computations can take place, stimuli first have to be parsed from the natural world,  
44 an environment where most reward predicting events are perceptually complex. This suggests that sensory  
45 processing might be an important integral part of optimized value-based decision-making.  
46 Here, we investigate whether choice outcomes can modulate the early sensory processing of perceptually  
47 complex stimuli to help bias future decisions. Recent neurophysiological studies find visually responsive  
48 neurons in the tail of the caudate nucleus, which is part of the dorsal striatum (Kim and Hikosaka 2013;  
49 Hikosaka et al. 2014). These neurons encode and differentiate stable reward values of visual objects to  
50 facilitate eye movements towards the most valued target, while at the same time inhibiting a movement  
51 towards the lesser valued object (Kim et al. 2017). Critically, differential modulations are also observed in the  
52 primary visual cortex where stronger cortical responses are seen for objects with higher values (Serences 2008;  
53 Serences and Saproo 2010), which is consistent with the response of visual neurons in the caudate. As visual  
54 cortex is densely connected to the striatum (Fernandez-Ruiz et al. 2001; Kravitz et al. 2013), prioritized  
55 visual processing of high-value stimuli could aid the integration of information regarding the most-valued  
56 choice in the striatum (Lim et al. 2011, 2013; Jahfari et al. 2015; Jahfari and Theeuwes 2017). To understand  
57 these visual-striatal interactions, we focus on a more detailed parsing of the underlying computations.

58 Specifically, we explored two questions by reanalyzing fMRI data from a probabilistic reinforcement learning  
59 task using faces as visual stimuli (Jahfari et al. 2018) (Figure 1a). First, we focus on the interplay between  
60 learning and visual activity in the fusiform face area (FFA) and occipital cortex (OC). Here, with the use of  
61 a Bayesian hierarchical reinforcement learning model (Figure 1b) we outline how trial-by-trial estimates of  
62 action values ( $Q$ -value) and reward prediction errors (RPE) relate to the BOLD response of visual regions  
63 and the striatum (O'Doherty et al. 2007; Daw 2011) (Figure 1c). Second, we analyze data from a follow-up  
64 transfer phase, where the learning of value was already established. In our analysis, the importance of  
65 visual brain activity in the prediction, or decoding, of future value-based decisions is evaluated by using a  
66 supervised Random Forest (RF) machine learning algorithm (Breiman 2001, 2004). Specifically, transfer  
67 phase single-trial BOLD estimates from anatomically defined visual, prefrontal, and subcortical regions are  
68 combined by RF to predict, or decode, choice outcomes in a separate validation set. We focus on classification  
69 accuracy, and the relative importance of each brain region in the correct classification of future value-based  
70 decisions.

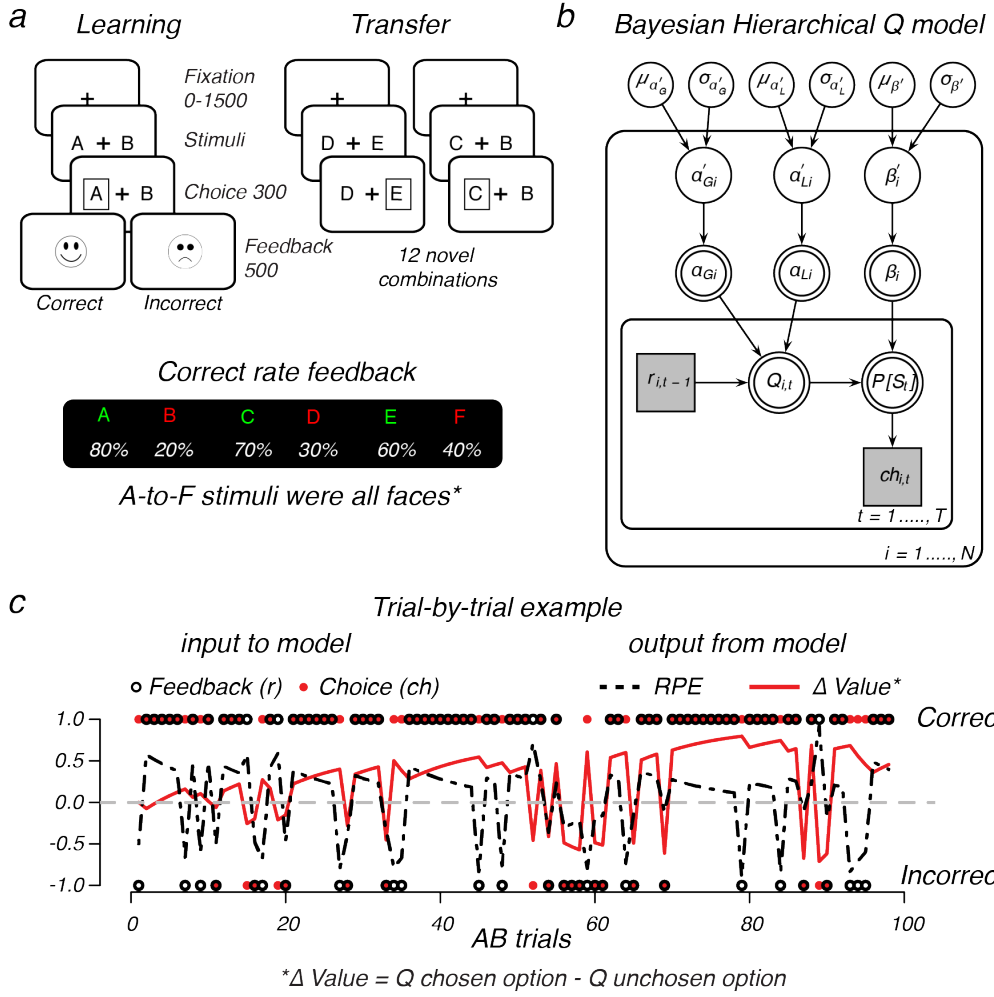


**Figure 1: Design and Model.** **a)** Reinforcement learning task using faces. During learning, two faces were presented on each trial, and participants learned to select the optimal face identity (A, C, E) through probabilistic feedback (% of correct is shown beneath each stimulus). The learning-phase contained three face pairs (AB, CD, ED) for which feedback was given. In a follow-up transfer phase these faces were rearranged into 12 novel combinations to assess learning. These trials were identical to learning trials, with the exception of feedback. \*Example faces were removed for the publication on BioRxiv, for an impression see Jahfari et al. (2018), or the Radboud face database from where the faces were originally selected (<http://www.socsci.ru.nl:8180/RaFD2/RaFD>). **b)** Graphical  $Q$ -learning model with hierarchical Bayesian parameter estimation. The model consists of an outer subject ( $i = 1, \dots, N$ ), and an inner trial plane ( $t = 1, \dots, T$ ). Nodes represent variables of interest. Arrows are used to indicate dependencies between variables. Double borders indicate deterministic variables. Continuous variables are denoted with circular nodes, and discrete with square nodes. Observed variables are shaded in grey (see methods for details about the fitting procedure). **c)** Illustration of the observed trial-by-trial input (i.e., the choice made, and feedback received), and output (i.e.,  $Q$  for the chosen and unchosen stimulus,  $\Delta$ Value, and RPE) of the model given the estimated variability in learning rates from either positive ( $\alpha_{G_i}$ ) or negative ( $\alpha_{L_i}$ ) feedback, and the tendency to exploit  $\beta$  higher values  $i$ .

## 71 Materials and Methods

72 To understand how value learning relates to the activity pattern in perceptual regions we reanalyzed the  
73 behavioral and fMRI recordings of a recent study (Jahfari et al. 2018). In this study, BOLD signals were  
74 recorded while participants performed a reinforcement learning task using male or female faces, and a  
75 stop-signal task (which was discussed in Jahfari et al. (2018)). The fusiform face area (FFA) was localized  
76 using a separate experimental run.

## 77 Participants

78 49 young adults (25 male; mean age = 22 years; range 19-29 years) participated in the study. All participants  
79 had normal or corrected-to-normal vision and provided written consent before the scanning session, in  
80 accordance with the declaration of Helsinki. The ethics committee of the University of Amsterdam approved  
81 the experiment, and all procedures were in accordance with relevant laws and institutional guidelines. In  
82 total, six participants were excluded from all analyses due to movement (2), incomplete sessions (3), or  
83 misunderstanding of task instructions (1). In total data from 43 participants was analyzed.

## 84 Reinforcement learning task

85 Full details of the reinforcement learning task are provided in Jahfari et al. (2018). In brief, the task consisted  
86 of two phases (Figure 1a). In the first learning phase, three male or female face pairs (AB, CD, EF) were  
87 presented in a random order, and participants learned to select the most optimal face (A, C, E) in each pair  
88 solely through probabilistic feedback ('correct': happy smiley, 'incorrect': sad smiley). Choosing face-A lead  
89 to 'correct' on 80% of the trials, whereas a choice for face-B only lead to the feedback 'correct' for 20% of the  
90 trials. Other ratios for 'correct' were 70:30 (CD) and 60:40 (EF). Participants were not informed about the  
91 complementary relationship in pairs. All trials started with a jitter interval where only a white fixation cross  
92 was presented and had a duration of 0, 500, 1000 or 1500ms to obtain an interpolated temporal resolution of  
93 500ms. Two faces were then shown left and right of the fixation-cross and remained on screen up to response,  
94 or trial end (4000ms). If a response was given on time, a white box surrounding the chosen face was then  
95 shown (300ms) and followed (interval 0-450ms) by feedback (500ms). Omissions were followed by the text  
96 'miss' (2000ms). The transfer-phase contained the three face-pairs from the learning phase, and 12 novel  
97 combinations, in which participants had to select which item they thought had been more rewarding during  
98 learning. Transfer-phase trials were identical to the learning phase, with the exception that no feedback was

99 provided. All trials had a fixed duration of 4000ms, where in addition to the jitter used at the beginning of  
100 each trial, null trials (4000ms) were randomly interspersed across the learning (60 trials; 20%) and transfer  
101 (72 trials; 20%) phase. Each face was presented equally often on the left or right side, and choices were  
102 indicated with the right-hand index (left) or middle (right) finger. Before the MRI session, participants  
103 performed a complete learning phase to familiarize with the task (300 trials with different faces). In the MRI  
104 scanner, participants performed two learning blocks of 150 trials each (300 trials total; equal numbers of AB,  
105 CD and EF), and three transfer phase blocks of 120 trials each (360 total; 24 presentations of each pair). All  
106 stimuli were presented on a black-projection screen that was viewed via a mirror-system attached to the MRI  
107 head coil.

## 108 Reinforcement learning model

109 Trial-by-trial updating in value beliefs about the face selected in the learning phase, and reward prediction  
110 errors (signed expectancy violations) were estimated with a variant of the computational *Q*-learning algorithm  
111 (Watkins and Dayan 1992; Frank et al. 2007; Daw 2011) that is frequently used with this reinforcement  
112 learning task and contains two separate learning rate parameters for positive ( $\alpha_{gain}$ ) and negative ( $\alpha_{loss}$ )  
113 reward prediction errors (Frank et al. 2007; Kahnt et al. 2009; Niv et al. 2012; Jahfari and Theeuwes 2017;  
114 Jahfari et al. 2018). *Q*-learning assumes participants to maintain reward expectations for each of the six  
115 (A-to-F) stimuli presented during the learning phase. The expected value (*Q*) for selecting a stimulus *i* (could  
116 be A-to-F) upon the next presentation is then updated as follows:

$$Q_i(t+1) = Q_i(t) + \begin{cases} \alpha_{Gain}[r_i(t) - Q_i(t)], & \text{if } r = 1 \\ \alpha_{Loss}[r_i(t) - Q_i(t)], & \text{if } r = 0 \end{cases}$$

117 Where  $0 \leq \alpha_{gain}$  or  $\alpha_{loss} \leq 1$  represent learning rates, *t* is trial number, and  $r = 1$  (positive feedback) or  $r = 0$   
118 (negative feedback). The probability of selecting one response over the other (i.e., A over B) is computed as:

$$P_A(t) = \frac{\exp(\beta * Q_t(A))}{\exp(\beta * Q_t(B)) + \exp(\beta * Q_t(A))}$$

119 With  $0 \leq \beta \leq 100$  known as the inverse temperature.

## 120 Bayesian hierarchical estimation procedure

121 To fit this  $Q$ -learning algorithm with two learning rate parameters we used Bayesian hierarchical estimation  
122 procedure. The full estimation procedure is explained in (Jahfari et al. 2018). To summarize, this  
123 implementation assumes that probit-transformed model parameters for each participant are drawn from  
124 a group-level normal distribution characterized by group level mean and standard deviation parameters:  
125  $z \sim N(\mu_z, \sigma_z)$ . A normal prior was assigned to group-level means  $\mu_z \sim N(0, 1)$ , and a uniform prior to the  
126 group-level standard deviations  $\sigma_z \sim U(1, 1.5)$ . Model fits were implemented in Stan, where multiple chains  
127 were generated to ensure convergence.

## 128 Image acquisition

129 The fMRI data for the Reinforcement learning task was acquired in a single scanning session with two learning  
130 and three transfer phase runs on a 3-T scanner (Philips Achieva TX, Andover, MA) using a 32-channel head  
131 coil. Each scanning run contained 340 functional  $T2^*$ -weighted echo-planar images for the learning phase,  
132 and 290  $T2^*$ -weighted echo planar images for the transfer phase (TR = 2000 ms; TE = 27.63 ms; FA =  
133 76.1°; 3 mm slice thickness; 0.3 mm slice spacing; FOV =  $240 \times 121.8 \times 240$ ; 80 × 80 matrix; 37 slices,  
134 ascending slice order). After a short break of 10 minutes with no scanning, data collection was continued  
135 with a three-dimensional  $T1$  scan for registration purposes (repetition time [TR] = 8.5080 ms; echo time  
136 [TE] = 3.95ms; flip angle [FA] = 8°; 1 mm slice thickness; 0 mm slice spacing; field of view [FOV] =  $240$   
137  $\times 220 \times 188$ ), the fMRI data collection using a stop signal task (described in Jahfari et al. (2018)), and  
138 a localizer task with faces, houses, objects, and scrambled scenes to identify FFA responsive regions on an  
139 individual level (317  $T2^*$  weighted echo-planar images; TR = 1500 msec; TE = 27.6 msec; FA = 70°; 2.5  
140 mm slice thickness; 0.25 mm slice spacing; FOV =  $240 \times 79.5 \times 240$ ; 96 × 96 matrix; 29 slices, ascending  
141 slice order). Here, participants viewed a series of houses, faces, objects as well as phase-scrambled scenes.  
142 To sustain attention during functional localization, subjects pressed a button when an image was directly  
143 repeated (12.5% likelihood).

## 144 fMRI analysis learning phase

145 The interplay between learning and perceptual activity was examined by evaluating how trial-by-trial  
146 computations of value-beliefs, and reward prediction errors relate to BOLD responses in the occipital cortex  
147 (OC) and fusiform face area (FFA). To compare perceptual responses with the more traditional literature, we

148 first show how value-beliefs and RPEs relate to the activity pattern of the dorsal (i.e., caudate, or putamen)  
149 or ventral (i.e., accumbens) parts of the striatum. Regions of interest (ROI) templates were defined using  
150 anatomical atlases available in FSL, or the localizer task for FFA. For this purpose, the localizer scans  
151 were preprocessed using motion correction, slice-time correction, and pre-whitening (Woolrich et al. 2001).  
152 For each subject, a GLM was fitted with the following EVs: for FFA, faces > (houses and objects), for  
153 parahippocampal place area (PPA), houses > (faces and objects) and for lateral occipital complex (LOC),  
154 intact scenes > scrambled scenes. Higher-level analysis was performed using FLAME Stage 1 and Stage  
155 2 with automatic outlier detection (Beckmann et al. 2003). For the whole-brain analysis Z (Gaussianized  
156 T/F) statistic images were thresholded using clusters determined by  $z > 2.3$  and  $p < .05$  (GRFT) to define  
157 a group-level binary FFA region. Templates used for the caudate [center of gravity (cog): (-) 13, 10, 10],  
158 putamen [cog: (-) 25, 1, 1], and nucleus accumbens [cog: (-)19, 12, -7] were based on binary masks. Because  
159 participants were asked to differentiate faces, for each participant, we multiplied the binary templates of OC  
160 [cog: 1, -83, 5], FFA [cog: 23, -48, -18] with the individual t-stats from the localizer task contrast faces >  
161 (houses and objects). All anatomical masks, and the localizer group-level FFA mask can be downloaded from  
162 github (see acknowledgements).

## 163 Deconvolution analysis learning phase

164 To more precisely examine the time course of activation in the striatal and perceptual regions, we performed  
165 finite impulse response estimation (FIR) on the BOLD signals. After motion correction, temporal filtering  
166 (3rd order savitzky-golay filter with window of 120 s) and percent signal change conversion, data from each  
167 region was averaged across voxels while weighting voxels according to ROI probability masks, and upsampled  
168 from 0.5 to 3 Hz. This allows the FIR fitting procedure to capitalize on the random timings (relative to  
169 TR onset) of the stimulus presentation and feedback events in the experiment. Separate response time  
170 courses were simultaneously estimated triggered on two separate events: stimulus onset, feedback onset. FIR  
171 time courses for all trial types were estimated simultaneously using a penalized (ridge) least-squares fit, as  
172 implemented in the FIRDeconvolution package (Knapen and Gee 2016), and the appropriate penalization  
173 parameter was estimated using cross-validation. For stimulus onset events (i.e., onset presentation of face  
174 pairs) response time courses were fit separately for the AB, CD and EF pairs, while also estimating the time  
175 courses of signal covariation with chosen and unchosen value for these pairs. For these events, our analysis  
176 corrected for the duration of the decision process. For the feedback events, the co-variation response time  
177 course with signed and unsigned prediction errors were estimated. These signal response time courses were  
178 analysed using across-subjects GLMs at each time-point using the statsmodels package (Seabold and Perktold

179 2010). The  $\alpha$  value for the contributions of  $Q$  or RPE was set to 0.0125 (i.e. a Bonferroni corrected value of  
180 0.05 given the interval of interest between 0 and 8 s).

## 181 Random Forest classification

182 To specify the relevance of perceptual regions in the resolve of future value-driven choices a random forest  
183 (RF) classifier was used (Breiman 2001, 2004). The RF classifier relies on an ensemble of decision trees as  
184 base learners, where the final prediction (e.g., for a given trial is the choice going to be correct/optimal? or  
185 incorrect/suboptimal? given past learning) is obtained by a majority vote that combines the prediction of  
186 all decision trees. To achieve controlled variation, each decision tree is trained on a random subset of the  
187 variables (i.e. regions of interest chosen), and a bootstrapped sample of data points (i.e. trials or rows of  
188 the matrix in Figure 2c). In the construction of each tree about 1/3 of all trials is left out - termed as the  
189 “out-of-bag” sample – and later used to see how well each tree preforms on unseen data in the training set.  
190 Because in RF each tree is built from a different sample of the original data each observation is “out-of-bag”  
191 (OOB) for some of the trees. As such, each OOB sample is offered to all trees where the sample was not  
192 used for construction, and the average vote across those trees is taken as the classification outcome. The  
193 proportion of times that the classification outcome is not equal to the actual choice is averaged over all cases  
194 and represents the RF OOB error estimate. In other words, the generalized error for predictions is calculated  
195 by aggregating the prediction for every out-of-bag sample across all trees. In the results section, the OOB  
196 errors obtained from RF during training were well matched with the classification accuracy seen for the  
197 validation set given only the ‘good learners’ (OOB=30%, RF error validation set= 31%) or all participants  
198 (OOB= 33%, RF error validation set= 35%). An important feature of the RF classification method is the  
199 ease to measure the relative importance of each variable (i.e., region), in the overall predictive performance.  
200 That is, it allows for the ranking of all regions evaluated in the prediction of future value-based decisions.

## 201 ROI selection and Random Forest procedure

202 This study used the ‘Breiman and Cutler’s Random Forests for Classification and Regression’ package in R,  
203 termed randomForest (randomForest\_4.6-14). RF evaluations relied on the fMRI data recorded during the  
204 transfer phase, in a set of 9 regions of interest (ROIs). These ROIs included all templates from the learning  
205 phase (i.e., caudate, putamen, accumbens, OC, and FFA), as well as, the ventromedial prefrontal cortex  
206 (vmPFC), dorsolateral prefrontal cortex (DLPFC), pre-supplementary motor area (preSMA), and the primary  
207 motor cortex (M1). The selection of these additional anatomical templates was inspired by our previous

208 analysis of this data with those templates focusing on networks (Pircalabelu et al. 2015; Schmittmann et  
209 al. 2015; Jahfari et al. 2018). Specifically, the DLPFC template was obtained from an earlier study, linking  
210 especially the posterior part to action execution (Cieslik et al. 2012). The preSMA, vmPFC, and M1 mask  
211 were created from cortical atlases available in FSL. Please notice that we used the same anatomical ROIs for  
212 both the model-based deconvolution analysis (Figure 4&5) and the decoding analysis (Figure 2&6). From each  
213 ROI a single parameter estimate (averaged normalized  $\beta$  estimate across voxels in each ROI) was obtained  
214 per trial, per subject. All, pre-processing steps to obtain single-trial images are described in Jahfari et  
215 al. (2018). Single-trial activity estimates were used as input variables in RF to predict choice outcomes  
216 (optimal/sub-optimal) in the transfer phase. Here, participants choose the best/optimal option based on  
217 values learned during the learning phase. We defined optimal choices as correct (i.e., when participants choose  
218 the option with the higher value), and sub-optimal choices as incorrect. Misses were excluded from RF  
219 evaluations.

220 By design, the transfer-phase contained 360 trials including 15 different pairs (12 novel), where each pair was  
221 presented 24 times with the higher value presented left in 12 of the 24 presentations, and on the right for the  
222 other half. With so many subtle value differences across the options presented and only one BOLD estimate  
223 per trial/region the prediction of future choices is under powered (Figure 2a). Therefore, assuming that all  
224 participants come from the same population, a fixed effects approach was taken for evaluations with RF.  
225 Here, the trial\*region activity matrices for all participants were combined into one big data matrix (Figure  
226 2b) and subsequently shuffled across the rows, so that both participants and trials were re-arranged in a  
227 random order across rows. Besides the single trial BOLD estimates from the 9 ROI's, this shuffled matrix  
228 contained two additional columns, which specified subject\_id (to which subject does each trial belong), and  
229 Trial Sign – i.e., is the choice between the two faces about two positive (+/++; AC, AE, CE), negative (-/-;  
230 BD, BF, DF), or a positive-negative (+/-; e.g. AD, CF etc. ) associations given the task manipulation during  
231 learning. Subject\_id was included to control for different BOLD fluctuations across participants, whereas  
232 Trial Sign was added because both BOLD and choice patterns differ across these options (please see Jahfari et  
233 al. (2018)). The shuffled fixed effect matrix was divided into a separate training (2/3 of whole matrix), and  
234 validation (1/3) set, to be used for RF evaluations (Figure 2c). Based on our previous connectivity work with  
235 this data (Jahfari et al. 2018), we were aware that many of our single-trial BOLD response were correlated  
236 across time, which potentially results from shared learning effects (Supplementary figure 4). With RF the  
237 problem of correlated features is minimized for predictions with variable selection - i.e., the random selection  
238 of a set of regions to use for each tree. With more variables selected, we get better splits in each tree but also  
239 highly correlated decisions trees across the forest, which in essence diminishes the forest effect. To find the

240 best balance, this study optimized the number of variables to select with a tuning function using the OOB  
241 error estimate. Learning was based on the training set, using 2000 trees with the number of variables (regions)  
242 used by each tree optimized with the tuneRF function in R, and accordingly set to 5. For the construction of  
243 each tree about 1/3 of all trials is left out - termed as the out-of-bag sample – and later used to see how well  
244 each tree performs on unseen data. The generalized error for predictions is calculated by aggregating the  
245 prediction for every out-of-bag sample across all trees. Besides this out-of-bag approximation we evaluated  
246 the predictive accuracy of the whole RF on the separate unseen validation-set. We further reasoned that RF  
247 predictions can result from alternative BOLD patterns such as the buildup of a motor response, the ease of  
248 face distinctions, or to us alternative functional fluctuations. Therefore, prior to the evaluation of region  
249 importance (or ranking), we performed two control analysis ensuring that RF predictions are sensitive to  
250 the consistency of past learning, and the representation of  $\Delta Value$ . These are the evaluations comparing  
251 ‘good’ to ‘all’ learners, as well as, the relationship between  $\Delta Value$  and RF uncertainty. In addition, while  
252 potential confounds of collinearity on the RF ranking cannot be excluded, we tried to minimize this with the  
253 use of permutation importance. Here, by using the OOB samples the importance of each variable (region) is  
254 computed as the difference between the models baseline accuracy and the drop in overall accuracy caused  
255 by permuting that column (region). While being more slow, permutation importance is described as more  
256 robust in comparison to the default (gini) importance computation where only the uncertainty of predictions  
257 is evaluated (with no checks on accuracy fluctuations after region permutation). The single trial data used as  
258 input, the RF evaluation codes, and ROI templates can all be downloaded from the github link provided in  
259 acknowledgements.

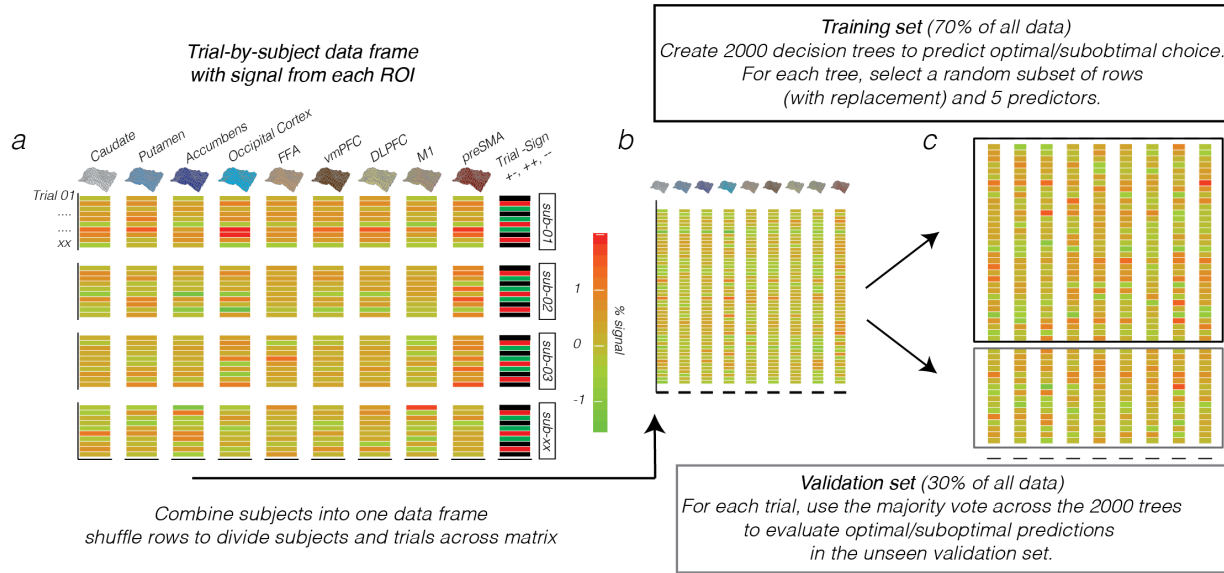


**Figure 2: Random Forest input and data-structure.** (a) Trial-by-subject data matrix with the % signal change drawn for each choice trial in the transfer-phase (rows) from 9 a-priori defined regions of interest (columns). In addition to the ROI data, the matrix contained a column with the identity of participants (sub-01, etc) and Trial Sign, which specified a choice between two positives (+/++; AC, AE, CE), negatives (-/-, BD, BF, DF), or between a negative and positive option (+/-, e.g., AD, CF, etc) given the feedback scheme in the learning-phase. (b) The individual subject data frames were then combined into one matrix, in which the rows were subsequently shuffled to randomly distribute trials and subjects across the rows. (c) This matrix was then divided into a training set (2/3 of the data) for the creation of 2000 decision trees of which the majority vote on each trial is then used to evaluate the predictive accuracy of optimal/suboptimal choices in a separate validation set (1/3 of the data).

260 Results

## **261 Model and Behavior**

262 As shown in Figure 1a, in the reinforcement learning task participants learned to select among choices with  
 263 different probabilities of reinforcement (i.e., AB 80:20, CD 70:30, and EF 60:40). A subsequent transfer phase,  
 264 where feedback was omitted, required participants to select the optimal option among novel pair combinations  
 265 of the faces that were used during the learning phase (Figure 1a). In the learning phase, subjects reliably  
 266 learned to choose the most optimal face option in all pairs. For each pair the probability of choosing the  
 267 better option was above chance ( $p$ 's < .001), and the effect of learning decreased from AB (80:20) and CD  
 268 (70:30) to the most uncertain EF (60:40) pair ( $F(2, 84) = 13.74, p < .0001$ ). At the end of learning, value  
 269 beliefs differentiating the optimal (A, C, E) from the sub-optimal (B, D, F) action were very distinct for  
 270 the AB and CD face pairs but decreased with uncertainty ( $F(2, 84) = 39.70, p < 0.0001$ , Figure 3a). Value

271 beliefs were estimated using the individual subject parameters of the  $Q$ -learning model that best captured  
 272 the observed data (Figure 3b-e; reproduced from Jahfari et al. (2018) to show performance).

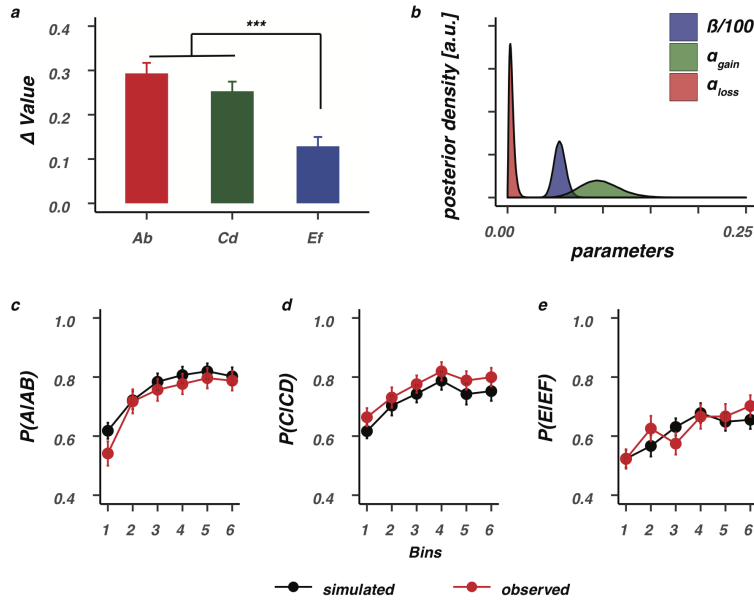


Figure 3: **Value differentiation and model performance.** (a) Value differentiation ( $\Delta$ Value) for the selection of the optimal (A,C,E) stimuli over the suboptimal (B,D,F) stimuli decreased as a function of feedback reliability, and was smallest for the most uncertain EF stimuli. \*\*\* =  $p < 0.0001$ , Bonferroni corrected. (b) Group-level posteriors for all  $Q$ -learning parameters. The bottom row shows model performance, where data was simulated with the estimated individual subject parameters and evaluated against the observed data for the AB (c), CD (d), or EF (e) pairs. Bins contain  $\pm 16$  trials. Error bars represent standard error of the mean (SEM).

273 **BOLD is modulated by reliable value differences between faces in striatal and  
 274 visual regions**

275 For each pair of faces presented during the learning phase (AB, CD, EF) we asked how the BOLD signal  
 276 time-course in striatal and visual regions relates to trial-by-trial value beliefs about the two faces presented  
 277 as a choice. First, as a reference, we focused on the activity pattern of three striatal regions. Results showed  
 278 BOLD responses in dorsal (caudate, putamen) but not ventral (accumbens) striatum to be differentially  
 279 modulated by the estimated value beliefs of the chosen face ( $Q_{chosen}$ ), in comparison to value beliefs about  
 280 the face that was not chosen ( $Q_{unchosen}$ ). Thus, BOLD responses in the dorsal striatum were modulated  
 281 more strongly by value beliefs about the chosen stimulus ( $Q_{chosen}$ ; Figure 4a bottom row). Critically, this  
 282 differential modulation was only observed with the presentation of AB faces where value differences were  
 283 most distinct because of the reliable feedback scheme. Next, we evaluated the relationship between value and  
 284 BOLD in the FFA, and OC. Again, only with the presentation of the AB face option, trial-by-trial BOLD

285 fluctuations were differentially modulated by values of the chosen versus not chosen face option (Figure  
 286 4b bottom row). These evaluations highlight how the BOLD response in striatal and perceptual regions is  
 287 especially sensitive to values of the (to-be) chosen stimulus when belief representations are stable and distinct.

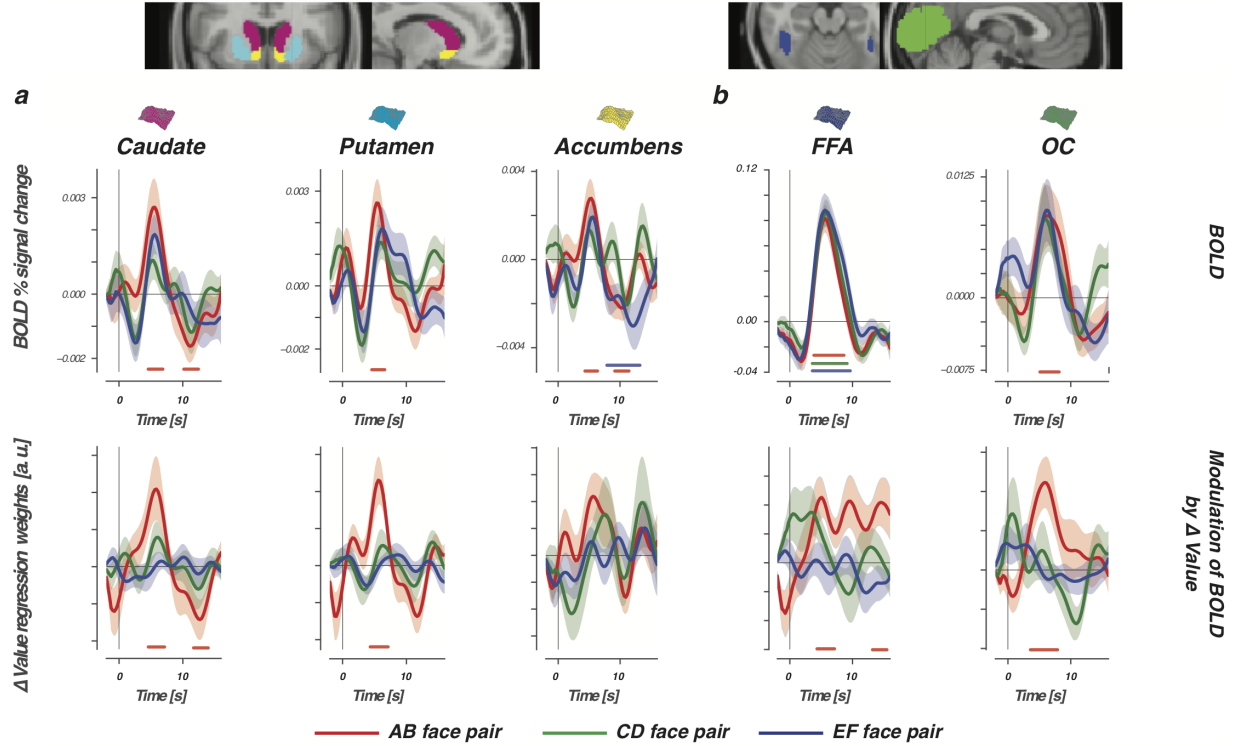


Figure 4: **BOLD and the modulation of  $\Delta$ Value in the learning phase.** Top row shows the BOLD signal course, time-locked to presentations of AB (80:20, red lines), CD (70:30, green lines), and EF (60:40, blue lines) face pairs, for three striatal regions (a) and two perceptual regions (b). Bottom row displays differential modulation by value ( $\Delta$ Value = modulation  $Q_{chosen}$  – modulation  $Q_{unchosen}$ ). Horizontal lines show the interval in which modulation was significantly stronger for  $Q_{chosen}$ . With the presentation of AB faces, BOLD responses in the dorsal striatum (caudate and putamen) and visual regions (FFA and OC) were modulated more by values of the chosen stimulus when compared to values of the unchosen stimulus. Differential AB value modulation was not significant in the ventral striatum (i.e., accumbens). Nor did we observe any differential value modulations with the presentation of the more uncertain CD and EF pairs. Confidence intervals were estimated using bootstrap analysis across participants ( $n = 1000$ ), where the shaded region represents the standard error of the mean across participants (bootstrapped 68% confidence interval).

288 **Reward prediction errors in striatal and visual regions**

289 Our findings so far described relationships between BOLD and value time-locked to the moment of stimulus  
 290 presentation – i.e., when a choice is requested. Learning occurs when an outcome is different from what  
 291 was expected. We therefore next focused on modulations of the BOLD response when participants received  
 292 feedback. Learning modulations were explored by asking how trial-by-trial BOLD responses in perceptual and

293 striatal regions relate to either signed (outcome was better or worse than expected) or unsigned (magnitude of  
 294 expected violation) reward prediction errors (Fouragnan et al. 2018). Consistent with the literature, BOLD  
 295 responses in all striatal regions were modulated by signed RPEs, with larger responses after positive RPEs or  
 296 smaller responses after negative RPEs (Figure 5a bottom row). Activity in the accumbens (ventral striatum)  
 297 was additionally tied to unsigned RPEs in the tail of the BOLD time-course, with larger violations (either  
 298 positive or negative) tied to smaller dips. Consistently, estimated BOLD responses in both visual regions  
 299 were modulated by the signed RPE, and once more mirrored the striatal modulations with stronger positive  
 300 RPEs eliciting stronger BOLD responses (Figure 5b bottom row). FFA BOLD responses were additionally  
 301 modulated by unsigned RPEs. However, in contrast to the relationship found between unsigned RPEs and  
 302 the accumbens, the FFA modulation was positive and co-occurred with the modulation of the signed RPE.  
 303 That is, bigger violations and more positive outcomes each elicited a stronger response in the FFA.

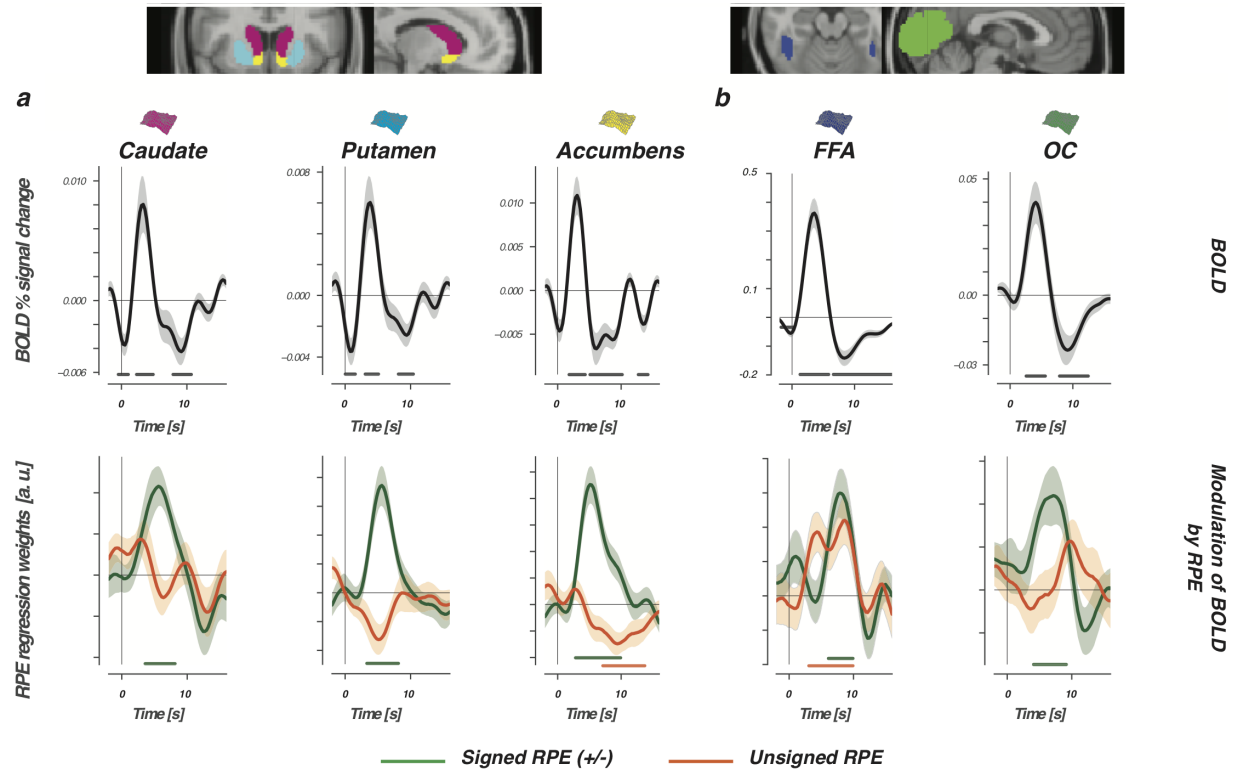


Figure 5: **Reward prediction errors modulate BOLD in striatal and visual regions.** The top row shows the FIR-estimated BOLD signal time-course, which was time-locked to the presentation of choice feedback and evaluated for three striatal regions (a) and two perceptual regions (b). Bottom row displays modulations of the estimated BOLD time-course by signed (green lines), or unsigned (orange lines) RPEs. The horizontal lines represent the interval in which signed or unsigned RPEs contributed significantly to the modulation of BOLD in the multiple regression. Note that both variables were always evaluated simultaneously in one GLM.

304 **Can past learning in visual regions support the prediction of future value-based  
305 decisions?**

306 Stable value representations and reward prediction errors both modulated the activity of visual and striatal  
307 regions. These modulations in the striatum are described to bias future actions towards the most favored  
308 option (the dorsal striatum), or to predict future reward outcomes (the ventral striatum). To better understand  
309 the value and RPE modulations observed in visual regions, we next assessed the importance of these visual  
310 regions alongside the striatum in the correct classification (decoding) of future value-driven choice outcomes.  
311 Here, activity of prefrontal regions was added to the importance evaluation based on our previous work with  
312 this data in the transfer phase (Jahfari et al. 2018) (please see supplementary Figures 1&2 for the evaluation  
313 of these regions during learning).

314 In the transfer phase, participants had to make a value-driven choice based on what was learned before, i.e.,  
315 during the learning phase. To specify the relevance of visual regions in the resolve of value-driven choice  
316 outcomes, in the transfer phase, a random forest (RF) classifier was used (Breiman 2001, 2004) (Please see  
317 Figure 2a-c for the procedure). The RF classifier was trained to predict the participant's choice, on each trial,  
318 given trial-by-trial BOLD estimates from striatal, prefrontal, and visual regions. The RF classifier relies on  
319 an ensemble of decision trees as base learners, where the prediction of each trial outcome is obtained by a  
320 majority vote that combines the prediction of all decision trees (Figure 6a). To achieve controlled variation,  
321 each decision tree is trained on a random subset of the variables (i.e. subset of columns shown in Figure 2a),  
322 and a bootstrapped sample of data points (i.e. trials). Importantly, we ensured that the forest was not simply  
323 learning the proportion of optimal choices in the transfer phase by training all models on balanced draws  
324 from the training set with equal numbers of optimal and sub-optimal choices.

325 Evaluation of all participants resulted in a classification accuracy of 65% ( $AUC = 0.75$ ) using the trial-by-trial  
326 BOLD estimates from the ROIs and increased to 70% with the evaluation of the good learners ( $AUC = 0.76$ ;  
327  $N = 34$ , criteria: accuracy  $> 60\%$  across all three learning pairs). Hence, in 65 (all participants) or 70 (good  
328 learners) out of 100 trials the forest correctly classified whether participants would pick the option with  
329 the highest value (optimal choice) or not (sub-optimal choice) in the validation set. RF predictions were  
330 substantially lower when labels of the validation set were randomly shuffled (accuracy: all participants= 52%;  
331 good learners= 56%).

332 The improvement of accuracy with the evaluation of only the good learners is remarkable because the  
333 classifier was given less data to learn the correct labelling (fewer subjects/trials) and implied that the 2000  
334 decision trees were picking up information related to the consistency of past learning. Further support

335 for this important observation was found by asking how the uncertainty of each prediction (defined as the  
336 proportion of agreement in the predicted outcome among the 2000 trees for each trial) relates to the difference  
337 in value beliefs ( $\Delta$ Value) about the two options presented on each trial (computed using the end  $Q_{beliefs}$   
338 of participants at the end of learning about face A-to-F), Figure 6c right side. As plotted in Figure 6c on  
339 the left, the uncertainty in predicting that a trial choice outcome is optimal – defined as the proportion of  
340 disagreement among the 2000 decision trees - decreased with larger belief differences in the assigned values  
341 (please see supplementary Figure 3 for the evaluation of all participants).

342 Besides providing insights into how BOLD responses in the transfer-phase contribute to predict value-driven  
343 choice outcomes (i.e., whether participants would choose the option with the highest value given past learning)  
344 the RF algorithm additionally outputs a hierarchy, thereby ranking the contribution of each region in the  
345 achieved classification accuracy. Figure 6d shows the ranking of all ROIs for good learners where the model  
346 had the highest predictive accuracy. First, regions in the dorsal striatum were most important, which aligned  
347 well with both the literature and the BOLD modulations we found by  $\Delta$ Value and RPE during the learning  
348 phase. These regions were next followed by the preSMA. Evaluation of this region during the learning  
349 phase showed no modulations by  $\Delta$ Value or RPE on BOLD (supplementary Figure 1&2). Nevertheless,  
350 this region is typically associated with choice difficulty/conflict and might be essential in the resolve of a  
351 choice when value differences are small. Remarkably, the third region in this hierarchy was the FFA. In  
352 a task where participants pick the most valued face based on past learning, this ranking of the FFA just  
353 above the vmPFC implies that the  $\Delta$ Value and RPE modulations of BOLD observed during learning could  
354 function to strengthen the recognition of valuable features. With the evaluation of all participants – including  
355 some who were less good in learning – the ranking of both the FFA and vmPFC was much lower (please see  
356 supplementary Figure 3b), which might be caused by more noise across the group in learning.

357 Further insights in the role of perceptual regions came from the separate evaluation of RF for only the  
358 easiest (with  $\Delta$ Value between the two choice options being large), or hardest (with small  $\Delta$ Value) choices  
359 (supplementary Figure 6). Results showed that when  $\Delta$ Value is large, or the choice is easy, RF predictions  
360 are best served by BOLD fluctuations in both dorsal and ventral striatum, followed by vmPFC, the preSMA  
361 and M1. With easy choices, regions involved with evidence accumulation (DLPFC), or perceptual processing  
362 (FFA and OC) rank last. More specifically, the processing of BOLD from OC even has a negative effect on  
363 RF accuracy, which means that running RF without OC will improve decoding. At the same time, with the  
364 evaluation of the most difficult choices - where participants decide between two very close in value positive  
365 (e.g., A or C) or negative (e.g., B or D) faces - we instead find perceptual regions to rank in the top. With  
366 difficult choices, where  $\Delta$ Value is very small, the caudate is followed by the FFA and OC in serving RF

367 predictions. We will return to the interpretation of these different rankings in the discussion.

368 Finally, we focused on two sets of control analysis. First, we evaluated RF accuracy and ranking with an  
369 additional random variable that was sampled from  $\mathcal{N}(0, 1)$ , and unrelated to the BOLD activity of any  
370 region, or  $\Delta$ Value. Here, the added random control region ranks last with negative importance, meaning that  
371 removing it improves model performance with 0.5% (good learners) or 0.3% (all learners) points (right side  
372 Figure 6d, or supplementary Figure 3). Second, RF performance was evaluated with the removal of perceptual,  
373 striatal, or frontal regions. Despite the positive ranking of each region shown in Figure 6d (or supplementary  
374 Figure 3b), RF decoding was not affected by the removal of just one or two regions (supplementary Figure  
375 5). However, accuracy is reduced when striatal (putamen, caudate, and accumbens), frontal (vmPFC, M1,  
376 DLPFC, and preSMA), or perceptual (FFA and OC) regions are evaluated in isolation. These alternative  
377 evaluations show that RF works best when trial-by-trial BOLD across multiple ‘learning’ brain regions is  
378 combined, but also that neither of the regions in isolation is crucial for the accuracy of predictions. Moreover,  
379 these control check highlight that when a variable is unrelated to learning, or single trial BOLD, ranking  
380 drops to last (as is to be expected) with counterproductive effects on RF accuracy.

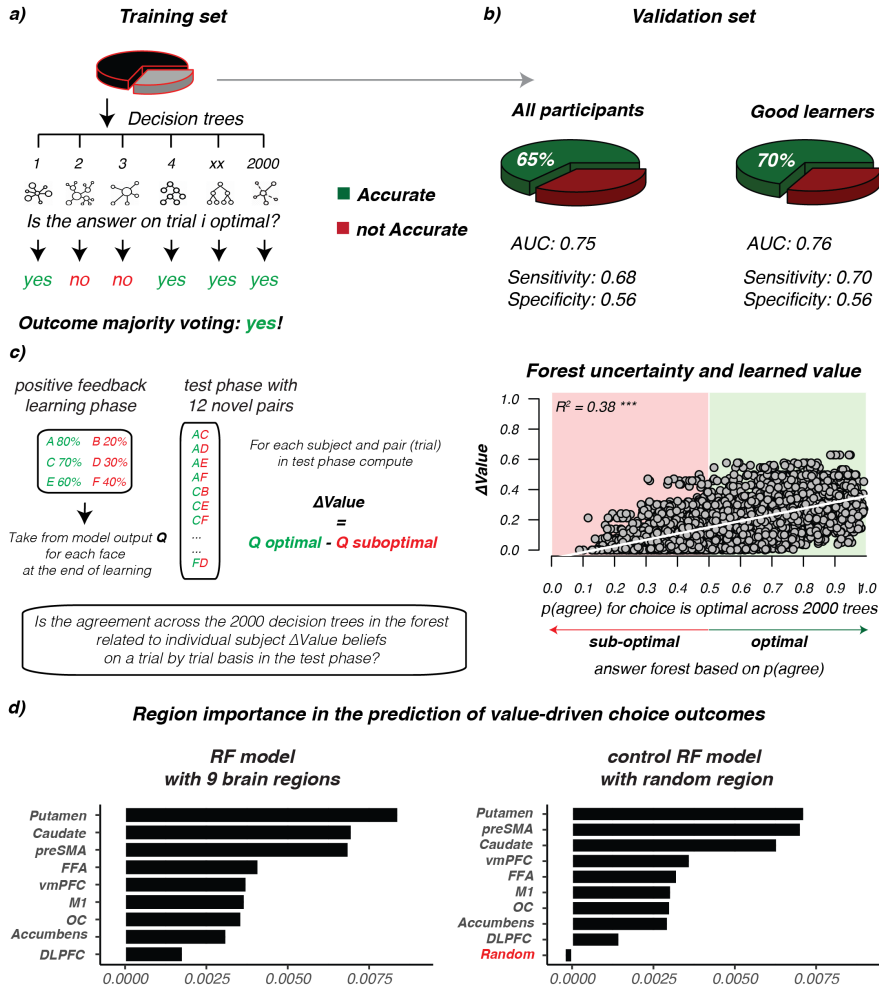


**Figure 6: Random Forest performance and importance ranking.** Prediction of value-driven choice outcomes in the transfer phase using trial-by-trial BOLD responses from striatal, perceptual, and prefrontal cortex regions. **(a)** Overview of the Random Forest approach where the training-set is used to predict choice outcomes for each trial by using the majority vote of 2000 different decision trees. Each tree is built using a different set, or sample, of trials and predictors from the training set. The forest is trained on a training set sampled from all participants ( $N=43$ ), or only ‘the good learners’ ( $N=34$ ). **(b)** Shows the classification, or decoding, accuracy (green) given the separate unseen validation sets, for all participants and good learners. **(c)** On the left, overview of the feedback scheme in the learning phase, and the new combination in transfer about which the RF is making an prediction with an illustration of how  $\Delta\text{Value}$  is computed for each trial.  $\Delta\text{Value}$  was computed for each trial in the transfer phase by using the end beliefs ( $Q$ ) that participants had about each stimulus (A-to-F) at the end of the learning phase. On the right side, plotted relationship between forest uncertainty (i.e., proportion of agreement across 2000 trees), on each prediction/trial (x-axis) and  $\Delta\text{Value}$  (y-axis) for the model with the highest accuracy (i.e., the good learners). Forest uncertainty is defined as the proportion of trees saying ‘yes! the choice on this trial was optimal/correct’. When this ratio is bellow 0.5 the forest will predict ‘no’ (sub-optimal/wrong choice), otherwise the prediction is ‘yes! the choice on this trial was optimal/correct’ (optimal).  $R^2$ =adjusted  $R^2$ . Note that, the same pattern was found for all participants ( $R^2=0.41^{***}$ , please see supplementary Figure 3). **(d)** Ranking of the ROI’s in their contribution to the predictive accuracy of the best performing model (i.e., good learners). Left, shows the original ranking. On the right, we evaluate ranking with all 9 original regions, but now add a control region that was sampled randomly from  $\mathcal{N}(0, 1)$ , and unrelated to the activity of any region, or  $\Delta\text{Value}$ . Notice that the random variable has negative importance in the ranking, meaning that removing it improves model performance with 0.5%.

## 381 Discussion

382 This study provides novel insights into how reinforcements modulate visual activity and specifies its potential  
383 in the prediction of future value-driven choice outcomes. First, by focusing on how participants learn, we find  
384 BOLD in visual regions to change with trial-by-trial adaptations in value beliefs about the faces presented,  
385 and then to be subsequently scaled by the signed RPE after feedback. Next, the relevance of these observed  
386 value and feedback modulations was sought by exploring the prediction of future value-driven choice outcomes  
387 in a follow-up transfer phase where feedback was omitted. Our machine learning algorithm here shows a  
388 classification accuracy of 70% for participants who were efficient in learning by combining trial-by-trial BOLD  
389 estimates from perceptual, striatal, and prefrontal regions. The evaluation of region importance in these  
390 predictions ranked the FFA just after the dorsal striatum and the preSMA, thereby showing an important  
391 role for visual regions in the prediction of future value-driven choice outcomes in a phase where learning is  
392 established.

393 In a choice between two faces, BOLD responses in both the dorsal striatum and perceptual regions were  
394 affected more by values of the chosen face, relative to the unchosen face. Across three levels of uncertainty,  
395 we only observed the differential modulation of value on BOLD when belief representations were stable.  
396 This specificity aligns with neuronal responses to perceptual stimuli in the caudate tail (Kim et al. 2017),  
397 visual cortex (Shuler and Bear 2006; Weil et al. 2010; Cicmil et al. 2015), and imaging work across sensory  
398 modalities (Serences 2008; Serences and Saproo 2010; LimOdoherty2013; Pleger et al. 2009; Kahnt et al.  
399 2011; Vickery et al. 2011; FitzGerald et al. 2013; Kaskan et al. 2016), where it fuels theories in which the  
400 learning of stable reward expectations can develop to modulate, or sharpen, the representation of sensory  
401 information critical for perceptual decision making (Roelfsema et al. 2010; Kahnt et al. 2011; Cicmil et al.  
402 2015).

403 After a choice was made, feedback modulations of signed ('valence') and unsigned ('surprise') RPEs (Fouragnan  
404 et al. 2018) were evaluated on BOLD responses, by using an orthogonal design where the unsigned and signed  
405 RPE compete to explain BOLD variances. Both visual and striatal regions respond to prediction errors  
406 (Den Ouden et al. 2012). In the striatum both valence and surprise are thought to optimize future action  
407 selection in the dorsal striatum, or the prediction of future rewards in the ventral striatum. In perceptual  
408 regions, a mismatch between the expected and received outcome is often explained as surprise where a boost  
409 in attention or salience changes the representation of an image without a representation of value per se. We  
410 found positive modulatory effects of signed RPEs in all striatal regions, as well as, in the FFA and OC.  
411 Concurrently, modulations of unsigned RPEs were only observed in the accumbens (ventral striatum) and

412 FFA, where notably the direction of modulation was reversed. We speculate that this contrast arises from the  
413 differential role of the regions. In the FFA, specialized and dedicated information processing is essential to  
414 quickly recognize valuable face features. Complementary boosts of surprise and valence here could prioritize  
415 attention towards the most rewarding face feature to strengthen the reward association in memory, or help  
416 speed up future recognition (Gottlieb 2012; Gottlieb et al. 2014; Störmer et al. 2014). In the accumbens,  
417 boosted effects of positive valence on BOLD were dampened by larger mismatches. Large mismatches in  
418 what was expected are rare in stable environments. We therefore reason that in the accumbens the contrast  
419 between valence and surprise could function as a scale to refine learning, eventually leading to more reliable  
420 predictions of future rewards.

421 Whereas BOLD in the ventral striatum was shaped by both signed and unsigned RPEs, the dorsal striatum  
422 was sensitive to differential value up-to a choice and signed RPEs with the presentation of feedback (Kaskan  
423 et al. 2016; Lak et al. 2016, 2017; McCoy et al. 2018; Van Slooten et al. 2018). The concurrent modulation  
424 of differential value in the primary motor cortex (please see M1 in supplementary Figure 1) associates the  
425 dorsal striatum with the integration of sensory information (Ding and Gold 2010; Yamamoto et al. 2012;  
426 Hikosaka et al. 2013; Kim et al. 2017), where increased visual cortex BOLD responses to faces with the  
427 highest value could potentially help bias the outcome of a value-driven choice.

428 We explored this line of reasoning with the prediction of value-driven choice outcomes in a follow-up transfer  
429 phase after leaning. In recent years, machine learning approaches have become increasingly important in  
430 neuroscience (Naselaris et al. 2011; Hassabis et al. 2017; Hebart and Baker 2018; Snoek et al. 2019), where  
431 the ease of interpretation has often motivated a choice for linear methods above non-linear methods (Naselaris  
432 et al. 2011; Kriegeskorte and Douglas 2018). Despite the latter being less constrained and able to reach a  
433 better classification accuracy by capturing non-arbitrary, or unexpected relationships (King et al. 2018).  
434 Value-driven choices after a phase of initial learning are influenced by the consistency of past learning, memory  
435 updating, and attention. All of these processes are affected by both linear and non-linear neurotransmitter  
436 modulations (Aston-Jones and Cohen 2005; Yu and Dayan 2005; Cools and D'Esposito 2011; Beste et al.  
437 2018). Our RF approach was unconstrained by linearity with classification accuracies well above chance and  
438 improved with the evaluation of only the good learners; despite substantial decreases in data given to the  
439 algorithm to learn the correct labelling. Critically, we additionally found that the uncertainty of trial-by-trial  
440 predictions made by RF is tied to the differentiability of value beliefs – an index that we could compute for  
441 the novel pair combination in the transfer phase by using the value ( $Q$ ) beliefs that participants had about  
442 each face at the end of learning. These results showcase how trial-by-trial BOLD fluctuations in striatal,  
443 prefrontal, and sensory regions can be combined by machine learning, or decoding, algorithms to reliably

444 predict the outcome of a value-driven choice. Where we refine the interpretation of non-linear predictions  
445 by combining the RF output with cognitive computational modelling. With this combination we essentially  
446 show how the uncertainty of RF predictions is tied to value beliefs acquired with learning in the past.

447 An important evaluation intended with our machine learning approach was the ranking of regions by their  
448 contribution to the predictive (decoding) accuracy in the transfer phase. After the observed modulations of  
449 BOLD in the learning phase this explorative analysis sought the relevance of learning-BOLD relationships in  
450 the resolve of future choices. Here, the ranking made by RF first identified signals from the dorsal striatum  
451 (putamen and caudate) as most important followed by the preSMA, and then most notably, visual regions.  
452 That is, when the quality of leaning was high across participants, FFA ranked just above traditional regions  
453 such as the vmPFC and the accumbens (O'Doherty et al. 2003, 2017; Hare et al. 2011; Niv et al. 2012; Klein  
454 et al. 2017). Notably, FFA was replaced by OC in ranking with the evaluation of all participants (please see  
455 supplementary Figure 3b). This difference could occur because the quality of learning was more variable  
456 across all participants, or because RF predictions based on the heterogeneous data from all participants were  
457 less accurate. In general, the shift in ranking implies that when learning is less consistent choice outcomes  
458 are better predicted by fluctuations in OC - perhaps with the identification of rewarding low-level features.  
459 With better or more consistent learning, however, participants should increasingly rely on memory and  
460 specialized visual areas. Thus, search for specific face features associated with high value by recruiting the  
461 FFA in the visual ventral stream. Consistent with this reasoning recent neuronal recordings show rapid visual  
462 processing of category-specific value cues in the ventral visual stream. These specific value cues are only  
463 seen for well-learned reward categories, and critically, precede the processing of value in prefrontal cortex  
464 (Sasikumar et al. 2018).

465 Additionally, in the learning phase both OC and the FFA were modulated more by values of the (to be) chosen  
466 stimulus when belief representations were stable and distinct - i.e., we only observed differential *Q*-value  
467 modulations for the most reliable and easy to learn AB pair. This combined with the RPE modulations found  
468 in the same regions suggests an effect of value and learning on perceptual regions that is both specialized  
469 (FFA) and global (OC). Note however that this possibility must be studied further with designs that can  
470 zoom in on specificity with the separation of different perceptual dimensions (e.g., houses vs faces). Our  
471 transfer phase results imply a differential role for the specialized FFA, and the more low-level general OC,  
472 with the comparison of good vs all learners. Tasked with predicting the outcome of future value-driven  
473 choices RF rankings showed a specialized and prominent FFA role for good/efficient learners whereas OC  
474 was more important with the evaluation of all participants (where learning was less consistent or noisier  
475 across participants). Recent work on the interplay between learning and attention suggests a bi-directional

476 relationship between learning and attention: we learn what to attend from feedback, and in turn, use selective  
477 attention to constrain learning towards relevant value dimensions (Leong et al. 2017; Rusch et al. 2017).  
478 In our study, better learning helps a more refined identification of rewarding features in a face, which we  
479 interpret as a narrower focus of selective attention in the FFA during learning (Niv et al. 2015). With past  
480 learning being more noisy, or less established, extraction of relevant features is less straightforward with  
481 attention being more spread to both specialized and global regions. Additionally, we observed both FFA and  
482 OC to only rank in the top (just after the caudate) when  $\Delta$ Value was very small (supplementary Figure 6).  
483 With easy choices this effect was reversed where processing of OC BOLD even declined the RF accuracy. This  
484 contrast suggests, that especially when the options to choose from are just too similar in value (i.e., think of  
485 the options A:C, or B:D), past learning in perceptual regions could serve the striatum with a selective boost  
486 to highlight the most rewarding face features. In contrast, when the distinction is easy and clear-cut, choices  
487 depend far more on inputs from the ventral striatum and vmPFC.  
488 We note that although BOLD fluctuations in the preSMA ranked second in the prediction of value-driven  
489 choice outcomes, no reliable modulations of BOLD were observed by either differential value or RPEs in  
490 the learning phase. The preSMA is densely connected to the dorsal striatum and consistently associated  
491 with action-reward learning (Jocham et al. 2016), or choice difficulty (Shenhav et al. 2014). The lack of  
492 associations in this study might result from our noisier estimates of the BOLD response that is typical  
493 for regions in the prefrontal cortex (Pircaabelu et al. 2015; Bhandari et al. 2018), the anatomical masks  
494 selected, or smaller variability across trials in the learning phase (i.e., 3 pairs in learning-phase vs 15 pairs  
495 in transfer-phase). Nevertheless, the importance indicated by RF, combined with our previous analysis of  
496 this transfer phase data (Jahfari et al. 2018), implies an important role for the preSMA in the resolve of  
497 value-driven choices in concert with the striatum. More research with optimized sequences to estimate BOLD  
498 in PFC is required to clarify the link between learning and transfer.  
499 To summarize, we find an important role for perceptual regions in the prediction of future value-driven choice  
500 outcomes, which coincides with the sensitivity of BOLD in visual regions to differential value and signed  
501 feedback. These findings imply visual regions to learn prioritize high value features with the integration of  
502 feedback, to support and fasten, optimal response selection via the dorsal striatum in future encounters.

## 503 Acknowledgements

504 This work was supported by an ABC Talent grant to SJ from the University of Amsterdam, an ERC grant  
505 ERC-2012-AdG-323413 to JT, and NWO-CAS grant 012.200.012 to TK.

## 506 Author contribution

507 SJ and TK developed the questions and analysis plan for the re-analysis. SJ and TK contributed novel  
508 methods and analyzed the data. SJ wrote the first draft of the MS with edits from TK. JT commented on  
509 the final draft.

## 510 Data availability

511 The code and preprocessed files for behavioral and decoding analyses can be download from: <https://github.com/sarajahfari/Pearl3T.git>, and fMRI preprocessing and deconvolution analysis code are available at  
512 [https://github.com/tknapen/pearl\\_3T](https://github.com/tknapen/pearl_3T). The raw data can be downloaded from openneuro.org in BIDS after  
513 acceptance of this MS.

## 515 References

516 Aston-Jones G, Cohen JD. 2005. An integrative theory of locus coeruleus-norepinephrine function: Adaptive  
517 gain and optimal performance. *Annu Rev Neurosci.* 28:403–450.

518 Atallah HE, Lopez-Paniagua D, Rudy JW, O'Reilly RC. 2007. Separate neural substrates for skill learning  
519 and performance in the ventral and dorsal striatum. *Nature neuroscience.* 10:126–131.

520 Beckmann CF, Jenkinson M, Smith SM. 2003. General multilevel linear modeling for group analysis in fmri.  
521 *Neuroimage.* 20:1052–1063.

522 Beste C, Adelhöfer N, Gohil K, Passow S, Roessner V, Li S-C. 2018. Dopamine modulates the efficiency of  
523 sensory evidence accumulation during perceptual decision making. *International Journal of Neuropsychophar-*  
524 *macology.*

525 Bhandari A, Gagne C, Badre D. 2018. Just above chance: Is it harder to decode information from human  
526 prefrontal cortex blood oxygenation level-dependent signals? *Journal of cognitive neuroscience.* 1–26.

527 Breiman L. 2001. Random forests. *Machine learning.* 45:5–32.

528 Breiman L. 2004. Consistency for a simple model of random forests.

529 Cicmil N, Cumming BG, Parker AJ, Krug K. 2015. Reward modulates the effect of visual cortical microstim-  
530 ulation on perceptual decisions. *Elife.* 4:e07832.

531 Cieslik EC, Zilles K, Caspers S, Roski C, Kellermann TS, Jakobs O, Langner R, Laird AR, Fox PT, Eickhoff  
532 SB. 2012. Is there “one” dlpc in cognitive action control? Evidence for heterogeneity from co-activation-based  
533 parcellation. *Cerebral cortex.* 23:2677–2689.

534 Collins AGE, Frank MJ. 2014. Opponent actor learning (opal): Modeling interactive effects of striatal  
535 dopamine on reinforcement learning and choice incentive. *Psychological review.* 121:337–366.

536 Cools R, D’Esposito M. 2011. Inverted-u-shaped dopamine actions on human working memory and cognitive  
537 control. *Biological psychiatry.* 69:e113–e125.

538 Daw ND. 2011. Trial-by-trial data analysis using computational models. *Decision making, affect, and learning:*  
539 *Attention and performance XXIII.* 23:3–38.

540 Daw ND, O’doherty JP, Dayan P, Seymour B, Dolan RJ. 2006. Cortical substrates for exploratory decisions  
541 in humans. *Nature.* 441:876–879.

542 Den Ouden HEM, Kok P, De Lange FP. 2012. How prediction errors shape perception, attention, and  
543 motivation. *Frontiers in psychology.* 3:548.

544 Ding L, Gold JI. 2010. Caudate encodes multiple computations for perceptual decisions. *Journal of*  
545 *Neuroscience.* 30:15747–15759.

546 Fernandez-Ruiz J, Wang J, Aigner TG, Mishkin M. 2001. Visual habit formation in monkeys with neurotoxic  
547 lesions of the ventrocaudal neostriatum. *Proceedings of the National Academy of Sciences.* 98:4196–4201.

548 Fitzgerald THB, Friston KJ, Dolan RJ. 2013. Characterising reward outcome signals in sensory cortex.  
549 *Neuroimage.* 83:329–334.

550 Fouragnan E, Retzler C, Philastides MG. 2018. Separate neural representations of prediction error valence  
551 and surprise: Evidence from an fMRI meta-analysis. *Human brain mapping.*

552 Frank MJ, Moustafa AA, Haughey HM, Curran T, Hutchison KE. 2007. Genetic triple dissociation reveals  
553 multiple roles for dopamine in reinforcement learning. *Proceedings of the National Academy of Sciences.*  
554 104:16311–16316.

555 Gottlieb J. 2012. Attention, learning, and the value of information. *Neuron.* 76:281–295.

556 Gottlieb J, Hayhoe M, Hikosaka O, Rangel A. 2014. Attention, reward, and information seeking. *Journal of*  
557 *Neuroscience.* 34:15497–15504.

558 Hare TA, Schultz W, Camerer CF, O’Doherty JP, Rangel A. 2011. Transformation of stimulus value  
559 signals into motor commands during simple choice. *Proceedings of the National Academy of Sciences.*

560 108:18120–18125.

561 Hassabis D, Kumaran D, Summerfield C, Botvinick M. 2017. Neuroscience-inspired artificial intelligence.

562 *Neuron*. 95:245–258.

563 Hebart MN, Baker CI. 2018. Deconstructing multivariate decoding for the study of brain function. *Neuroimage*.

564 180:4–18.

565 Hikosaka O, Kim HF, Yasuda M, Yamamoto S. 2014. Basal ganglia circuits for reward value–guided behavior.

566 *Annual review of neuroscience*. 37:289–306.

567 Hikosaka O, Yamamoto S, Yasuda M, Kim HF. 2013. Why skill matters. *Trends in cognitive sciences*.

568 17:434–441.

569 Jahfari S, Ridderinkhof KR, Collins AGE, Knapen T, Waldorp LJ, Frank MJ. 2018. Cross-task contributions

570 of frontobasal ganglia circuitry in response inhibition and conflict-induced slowing. *Cerebral Cortex*. bhy076.

571 Jahfari S, Theeuwes J. 2017. Sensitivity to value-driven attention is predicted by how we learn from value.

572 *Psychonomic bulletin & review*. 24:408–415.

573 Jahfari S, Waldorp L, Ridderinkhof KR, Scholte HS. 2015. Visual information shapes the dynamics of

574 corticobasal ganglia pathways during response selection and inhibition. *Journal of cognitive neuroscience*.

575 27:1344–1359.

576 Jocham G, Boorman E, Behrens T. 2016. Neuroscience of value-guided choice. *The Wiley Handbook on the*

577 *Cognitive Neuroscience of Learning*. 554–591.

578 Jocham G, Klein TA, Ullsperger M. 2011. Dopamine-mediated reinforcement learning signals in the striatum

579 and ventromedial prefrontal cortex underlie value-based choices. *Journal of Neuroscience*. 31:1606–1613.

580 Joel D, Niv Y, Ruppin E. 2002. Actor–critic models of the basal ganglia: New anatomical and computational

581 perspectives. *Neural networks*. 15:535–547.

582 Kahnt T, Heinze J, Park SQ, Haynes J-D. 2011. Decoding different roles for vmPFC and dlPFC in

583 multi-attribute decision making. *Neuroimage*. 56:709–715.

584 Kahnt T, Park SQ, Cohen MX, Beck A, Heinz A, Wräse J. 2009. Dorsal striatal–midbrain connectivity

585 in humans predicts how reinforcements are used to guide decisions. *Journal of Cognitive Neuroscience*.

586 21:1332–1345.

587 Kaskan PM, Costa VD, Eaton HP, Zemskova JA, Mitz AR, Leopold DA, Ungerleider LG, Murray EA. 2016.

588 Learned value shapes responses to objects in frontal and ventral stream networks in macaque monkeys.

589 Cerebral Cortex. 27:2739–2757.

590 Kim HF, Amita H, Hikosaka O. 2017. Indirect pathway of caudal basal ganglia for rejection of valueless  
591 visual objects. *Neuron*. 94:920–930.

592 Kim HF, Hikosaka O. 2013. Distinct basal ganglia circuits controlling behaviors guided by flexible and stable  
593 values. *Neuron*. 79:1001–1010.

594 King J-R, Gwilliams L, Holdgraf C, Sassenhagen J, Barachant A, Engemann D, Larson E, Gramfort A.  
595 2018. Encoding and decoding neuronal dynamics: Methodological framework to uncover the algorithms of  
596 cognition.

597 Klein TA, Ullsperger M, Jocham G. 2017. Learning relative values in the striatum induces violations of  
598 normative decision making. *Nature Communications*. 8:16033.

599 Knapen T, Gee J. 2016. FIRDeconvolution.

600 Kravitz DJ, Saleem KS, Baker CI, Ungerleider LG, Mishkin M. 2013. The ventral visual pathway: An  
601 expanded neural framework for the processing of object quality. *Trends in cognitive sciences*. 17:26–49.

602 Kriegeskorte N, Douglas PK. 2018. Interpreting encoding and decoding models. *arXiv preprint*  
603 *arXiv:181200278*.

604 Lak A, Nomoto K, Keramati M, Sakagami M, Kepcs A. 2017. Midbrain dopamine neurons signal belief in  
605 choice accuracy during a perceptual decision. *Current Biology*. 27:821–832.

606 Lak A, Stauffer WR, Schultz W. 2016. Dopamine neurons learn relative chosen value from probabilistic  
607 rewards. *Elife*. 5:e18044.

608 Leong YC, Radulescu A, Daniel R, DeWoskin V, Niv Y. 2017. Dynamic interaction between reinforcement  
609 learning and attention in multidimensional environments. *Neuron*. 93:451–463.

610 Lim S-L, O'Doherty JP, Rangel A. 2011. The decision value computations in the vmPFC and striatum use a  
611 relative value code that is guided by visual attention. *Journal of Neuroscience*. 31:13214–13223.

612 Lim S-L, O'Doherty JP, Rangel A. 2013. Stimulus value signals in ventromedial pfc reflect the integration  
613 of attribute value signals computed in fusiform gyrus and posterior superior temporal gyrus. *Journal of*  
614 *Neuroscience*. 33:8729–8741.

615 McCoy B, Jahfari S, Engels G, Knapen T, Theeuwes J. 2018. Dopaminergic medication reduces striatal  
616 sensitivity to negative outcomes in parkinson's disease. *bioRxiv*.

617 Montague PR, Dayan P, Sejnowski TJ. 1996. A framework for mesencephalic dopamine systems based on  
618 predictive hebbian learning. *Journal of neuroscience*. 16:1936–1947.

619 Naselaris T, Kay KN, Nishimoto S, Gallant JL. 2011. Encoding and decoding in fMRI. *Neuroimage*.  
620 56:400–410.

621 Niv Y, Daniel R, Geana A, Gershman SJ, Leong YC, Radulescu A, Wilson RC. 2015. Reinforcement learning  
622 in multidimensional environments relies on attention mechanisms. *Journal of Neuroscience*. 35:8145–8157.

623 Niv Y, Edlund JA, Dayan P, O'Doherty JP. 2012. Neural prediction errors reveal a risk-sensitive reinforcement-  
624 learning process in the human brain. *Journal of Neuroscience*. 32:551–562.

625 O'Doherty J, Critchley H, Deichmann R, Dolan RJ. 2003. Dissociating valence of outcome from behavioral  
626 control in human orbital and ventral prefrontal cortices. *Journal of neuroscience*. 23:7931–7939.

627 O'Doherty J, Dayan P, Schultz J, Deichmann R, Friston K, Dolan RJ. 2004. Dissociable roles of ventral and  
628 dorsal striatum in instrumental conditioning. *Science*. 304:452–454.

629 O'Doherty JP, Cockburn J, Pauli WM. 2017. Learning, reward, and decision making. *Annual review of*  
630 *psychology*. 68:73–100.

631 O'Doherty JP, Hampton A, Kim H. 2007. Model-based fMRI and its application to reward learning and  
632 decision making. *Annals of the New York Academy of sciences*. 1104:35–53.

633 Pircalabelu E, Claeskens G, Jahfari S, Waldorp LJ. 2015. A focused information criterion for graphical  
634 models in fMRI connectivity with high-dimensional data. *The Annals of Applied Statistics*. 9:2179–2214.

635 Pleger B, Ruff CC, Blankenburg F, Klöppel S, Driver J, Dolan RJ. 2009. Influence of dopaminergically  
636 mediated reward on somatosensory decision-making. *PLoS biology*. 7:e1000164.

637 Roelfsema PR, Ooyen A van, Watanabe T. 2010. Perceptual learning rules based on reinforcers and attention.  
638 *Trends in cognitive sciences*. 14:64–71.

639 Rusch T, Korn CW, Gläscher J. 2017. A two-way street between attention and learning. *Neuron*. 93:256–258.

640 Sasikumar D, Emeric E, Stuphorn V, Connor CE. 2018. First-pass processing of value cues in the ventral  
641 visual pathway. *Current Biology*. 28:538–548.

642 Schmittmann VD, Jahfari S, Borsboom D, Savi AO, Waldorp LJ. 2015. Making large-scale networks from  
643 fMRI data. *PloS one*. 10:e0129074.

644 Schultz W, Dayan P, Montague PR. 1997. A neural substrate of prediction and reward. *Science*. 275:1593–

645 1599.

646 Seabold S, Perktold J. 2010. Statsmodels: Econometric and statistical modeling with python. In: Proceedings  
647 of the 9th python in science conference. p. 57–61.

648 Serences JT. 2008. Value-based modulations in human visual cortex. *Neuron*. 60:1169–1181.

649 Serences JT, Saproo S. 2010. Population response profiles in early visual cortex are biased in favor of more  
650 valuable stimuli. *Journal of neurophysiology*. 104:76–87.

651 Shenhav A, Straccia MA, Cohen JD, Botvinick MM. 2014. Anterior cingulate engagement in a foraging  
652 context reflects choice difficulty, not foraging value. *Nature neuroscience*. 17:1249.

653 Shuler MG, Bear MF. 2006. Reward timing in the primary visual cortex. *Science*. 311:1606–1609.

654 Snoek L, Miletic S, Scholte HS. 2019. How to control for confounds in decoding analyses of neuroimaging  
655 data. *NeuroImage*. 184:741–760.

656 Störmer V, Eppinger B, Li S-C. 2014. Reward speeds up and increases consistency of visual selective attention:  
657 A lifespan comparison. *Cognitive, Affective, & Behavioral Neuroscience*. 14:659–671.

658 Tobler PN, Fiorillo CD, Schultz W. 2005. Adaptive coding of reward value by dopamine neurons. *Science*.  
659 307:1642–1645.

660 Van Slooten JC, Jahfari S, Knapen T, Theeuwes J. 2018. How pupil responses track value-based decision-  
661 making during and after reinforcement learning. *PLoS computational biology*. 14:e1006632.

662 Vickery TJ, Chun MM, D L. 2011. Ubiquity and specificity of reinforcement signals throughout the human  
663 brain. *Neuron*. 72:166–177.

664 Watkins CJCH, Dayan P. 1992. Q-learning. *Machine learning*. 8:279–292.

665 Weil RS, Furl N, Ruff CC, Symmonds M, Flandin G, Dolan RJ, Driver J, Rees G. 2010. Rewarding feedback  
666 after correct visual discriminations has both general and specific influences on visual cortex. *American  
667 Journal of Physiology-Heart and Circulatory Physiology*. 104:1746–1757.

668 Woolrich MW, Ripley BD, Brady M, Smith SM. 2001. Temporal autocorrelation in univariate linear modeling  
669 of fMRI data. *Neuroimage*. 14:1370–1386.

670 Yamamoto S, Monosov IE, Yasuda M, Hikosaka O. 2012. What and where information in the caudate tail  
671 guides saccades to visual objects. *Journal of Neuroscience*. 32:11005–11016.

672 Yu AJ, Dayan P. 2005. Uncertainty, neuromodulation, and attention. *Neuron*. 46:681–692.